17th World Conference on Earthquake Engineering, 17WCEE
Sendai, Japan - September 13th to 18th 2020

SIMULTANEOUS LOW AND HIGH FREQUENCY BANDS INVERSION OF SEISMIC WAVEFORM

N. Umeda[(1)], Y. Sato[(2)]

[(1)] *Associate Chief Researcher, Research & Development Institute, Takenaka Corporation, umeda.naoko@takenaka.co.jp*
[(2)] *Group Leader, Research & Development Institute, Takenaka Corporation, satou.yoshiyukia@takenaka.co.jp*

Abstract

Waveform inversion is used to estimate fault slips in low-frequency bands and has recently been extended to high-frequency bands to elucidate heterogeneous slips. However, fitting the observed and calculated waveforms is generally unsatisfactory close to the upper frequency limit. This means a fine source image may not be reliably estimated. This study tests a method to better fit waveforms up to 1 Hz (which is generally the upper limit frequency for inversion analysis). We investigated waveform inversion using the theoretical Green's function. Since insufficient fitting is caused from the difference between the observed and calculated waveforms at high-frequency, we focused on the effect of the least squares method. By reducing the error, the low-frequency component is dominant, which determines the general shape of the waveform. As a result, there is a relatively reduced contribution from the high-frequency component. Therefore, we divided the analysis frequency into lower and higher bands, inverting these bands concurrently. The lower frequency band was up to 0.5 Hz, and the higher frequency band was from 0.5–1.0 Hz. As such, equal treatment of the low- and high-frequency components was expected in the least squares evaluation. Despite the independent handling of the two frequency bands, it was important to consider that these bands were generated from the same fault slip. For this reason, lower and higher frequency slip velocity functions were formed to generate Green's functions by assuming the ratio of equivalent slip of the higher frequency component to the lower frequency component based on Nakamura and Miyatake [1].

Employing this method, we performed waveform inversion for the 2016 Kumamoto earthquake using velocity records from 22 stations of the National Research Institute for Earth Science and Disaster Resilience Kyoshin Network and Kiban Kyoshin network (KiK-net) within the hypocenter distance of 100 km. Inversion was conducted using the two-band and the normal methods. Comparison of the band pass filtered waveforms from 0.5–1.0 Hz, showed that the division method better fitted observed waves for approximately one third of the stations. For example, the S-wave part amplitude was underestimated for all three components using the normal method at the KiK-net Mashiki station, but this difference was relatively reduced using the division method. This indicates that the division method may be more reliable for higher frequency data than its one-band counterpart. The effect of the 0.5–1.0 Hz component on the inferred fault slip was also examined, comparing the slip by the division and normal methods up to 1.0 and 0.5 Hz, respectively. Although overall slip distribution for both was similar, some small-scale slip regions were evident using the division method. These small-scale slip were distributed around the asperity. This pattern corresponds to one of the proposed images of high-frequency sources in previous studies. As such, dividing analysis frequency into two frequency bands may be effective for waveform inversion including the higher frequency component.

Keywords: waveform inversion; fault slip; high-frequency; 2016 Kumamoto earthquake

1. Introduction

Fault slip distribution estimated by waveform inversion is important to predict strong ground motion. To carry out this prediction, an understanding of broadband fault slip distribution is required. However, waveform inversion is generally performed at the low frequencies. The reason is that the fitting of the observed wave and the calculated wave at high-frequency is considered to become inferior compared with the fitting at low-frequency. The deterioration may stem from the lowering of the accuracy of Green's function because the underground model doesn't have enough fineness to compute the high-frequency component.

Nevertheless, recently, analysis has been extended to higher frequencies with some research findings available on high-frequency source images. For example, Miyake [2] used phase and amplitude spectra as targets for inversion up to 4 Hz and developed a broadband inversion method by changing each weight depending on the frequency. She found that the high-frequency source area was distributed around the low-frequency source area. Shiba [3] used a fast annealing method that was effective in acquiring an optimal solution for strong nonlinear problems for inversion up to 5 Hz. He claimed that the low-frequency and high-frequency sources were distributed in the same region. These examples indicate that conclusions on the distribution of the high-frequency source area remain unclear. To study this issue, it is necessary to improve the fitting of waveform inversion at high-frequency.

In this study, we focus on the least squares method itself, from another point of view. To minimize the error in the least squares method for a broadband range, it is necessary to make the waveform fitting to observed wave at a high-frequency precisely as at low-frequency. Therefore, we propose a method of dividing observation data into high-frequency and low-frequency components and inverting them in parallel. Moreover, we confirm the effect of the proposed method by comparing the result with the result of the normal method in which there is no dividing of frequencies.

2. Data

The earthquake used for the waveform inversion was the 2016 Kumamoto earthquake (M_{JMA} 7.3) that occurred on April 16, 2016. We used records of 22 stations in the Kyoshin (K-NET) and Kiban Kyoshin (KiK-net) networks of the National Research Institute for Earth Science and Disaster Resilience (NIED) [4]. Green's function was calculated using the wave number integration method by Hisada [5]. PS logging by NIED was used for the shallow ground while the Japan Seismic Hazard Information Station (J-SHIS) data [5] were used for deep ground. KiK-net Mashiki station (KMMH16) was close to the hypocenter, where large amplitude acceleration records were observed. KMMH16 is one of the most important stations for waveform inversion, yet, there was a large difference between the theoretical transfer function—based on the ground of J-SHIS and the observed transfer function. Therefore, we used the underground model modified by Umeda et al. [7].

Fig. 1 shows the assumed fault plane based on Asano and Iwata [8]. It consists of two faults; the Futagawa fault on the northeast side and the Hinagu fault on the southwest side. The Futagawa fault has a length of 28 km and a width of 18 km, and the Hinagu fault has a length of 14 km and a width of 18 km. Each fault was divided into 2 km × 2 km sub faults. The strike of the Futagawa fault was set at 235° with the dip angle set at 65°. The strike of the Hinagu fault was set at 205° with the dip angle set at 72°.

The rupture start point was set at a depth of 12.45 km with the rupture starting concentrically. The rake angle of the slip vector on each subfault was limited to ± 45° of the -142° slip angle of the F-net mechanism solution by NIED. The slip distribution was determined by the multiple-time-window linear waveform inversion based on Hartzell and Heaton [9].

The rupture velocity (Vr) was set to 2650 m/s at 0.72 times S-wave velocity (Vs), as per Geller [10]. The analyzed record was a velocity waveform of 30 s length clipped from 1s before the arrival of the S-wave. Since the accuracy of the underground structure was not considered, the upper limit of the reliable frequency was assumed at approximately 1 Hz. Therefore, in this study, we set the range of analysis frequency 0.05–1.0 Hz.

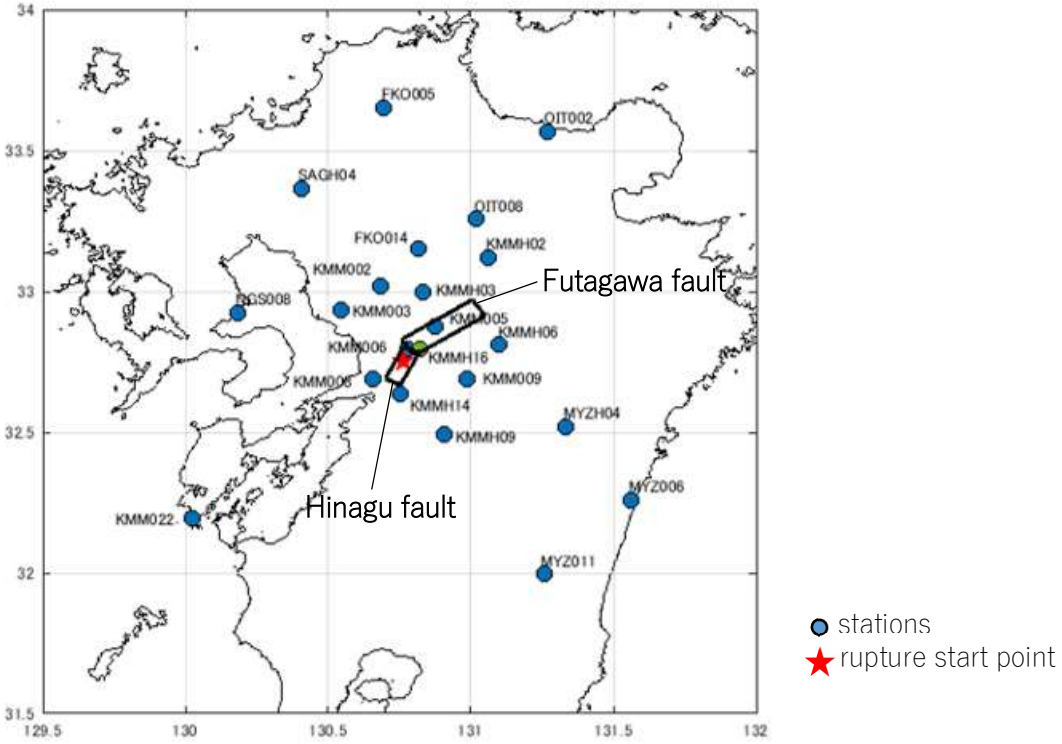

Fig. 1 – Faults of the 2016 Kumamoto earthquake and the stations in this study

3. Method

We used two methods for this study; the normal method and the division method. In the normal method, Fig. 2(a), the observed and calculated wave were filtered at 0.05 to 1.0 Hz. For the division method, Fig. 2(b), two types of filters, 0.05–0.5 Hz and 0.5–1.0 Hz, were applied to the observed and calculated wave, and these were inverted in parallel.

Fig. 3(a) shows that slip velocity functions for each small fault in the normal method were set with nine triangular functions, and a rise time of 1 s shifted by 0.5 s. However, it may be difficult for the broadband theoretical waveform to correspond to the observed waveform as it is difficult to generate broadband ground motions by using one kind of slip velocity time function. Therefore, different slip velocity time functions of 0.05–0.5 Hz (low-frequency part) and 0.5–1.0 Hz (high-frequency part) were used in the division method. We also devised improvements to the fitting of the waveform in the low and high-frequency. For low-frequency, we used the same triangular functions as the normal method shown in Fig. 3 (b). For high-frequency, we used nine triangular functions with a rise time of 0.4 s by shifting by 0.2 s shown in Fig. 3 (c).

For the division method, the low-frequency and high-frequency components were generated from the same sub fault slip through two different slip velocity time functions. The ratio of the low to high-frequency slip was determined based on the slip velocity time function proposed by Nakamura and Miyatake [1]. Fig. 3 shows the slip velocity time function by Nakamura and Miyatake [1]. The parameter ‘tb’ shows the boundary between a sharp slip in the first half and a stable slip in the second half. It was assumed that the slip from 0 to tb corresponds to the slip at high-frequency. It was assumed that slips from tb to 3.5 tb corresponded to low-frequency slips. Multiplying by 3.5 was decided based on the ratio of the width of the triangular function between high and low-frequency. The ratio of the low- and high-frequency trigonometric functions was determined from the area ratio of each section described above. From these area ratios, the slip ratio of high to low-frequency was assumed at 0.81:1. Using this ratio, Green's function of the division method was calculated.

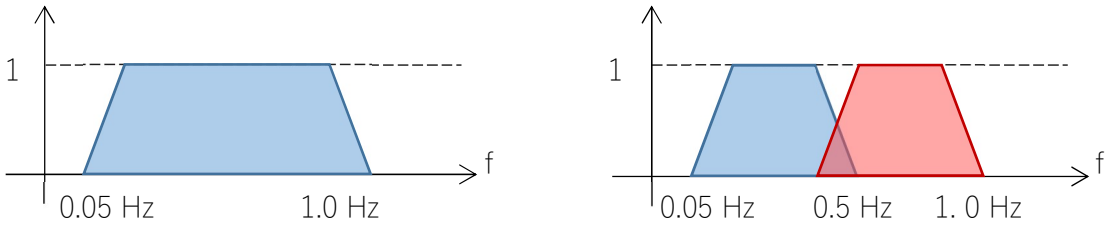

(a) normal method (b) division method

Fig. 2 – Conceptual diagram of frequency filter

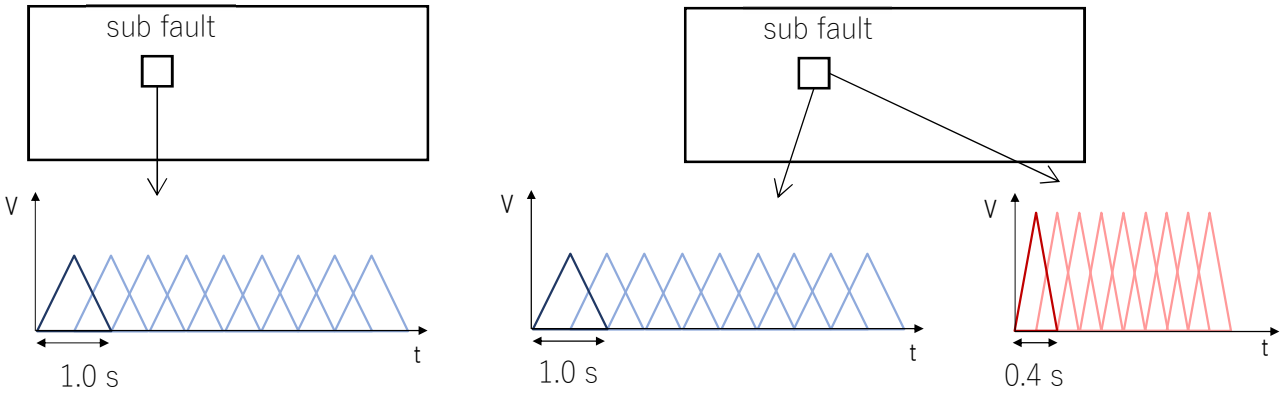

(a) normal method (b) low frequency part (division method) (c) high frequency part (division method)

Fig. 3 – Slip velocity time function

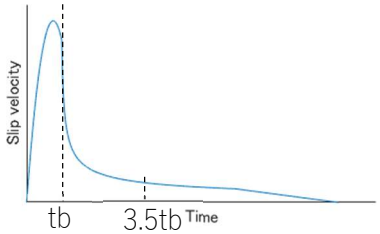

Fig. 4 – Slip velocity time function by Nakamura and Miyatake [1]

4. Results

The results from the normal and division methods were compared between 0.05 to 1.0 Hz. Fig. 5 shows an example of fitting between observed and calculated velocity waves. The amplitude of the waveform is shown normalized to the same amplitude at each station in all frequency ranges. However, for KMMH16, the amplitude of the high-frequency was smaller than the amplitude of the other frequency bands. Therefore, we plotted the amplitude of the high-frequency component as three times that of other frequencies for only KMMH16 to clarify the difference between the methods. The residuals from the waveform inversion of the division method are reduced by approximately 4% compared with the normal method.

Fig. 6 shows the ratio of the residual sum of squares (RSS) of the division method to the normal method at each observation point for each frequency band. That is, when the RSS of the division method is smaller than the normal method, the RSS ratio shows a value smaller than 1.0. Stations are arranged from left to right in order of proximity to the hypocenter. For 0.05–0.5 Hz, most stations show around unity, and the difference between the two methods was small. On the other hand, for 0.5–1.0 Hz, at 11 stations out of all 22 stations the

ratio has decreased below 0.9. This means that the fitting to observed waves for 0.5–1.0 Hz is improved by the division method. At stations where the hypocentral distance is relatively short, it seems that the degree of the improvement is large. For especially KMMH16, where the highest seismic intensity of 7 was observed, the residual of the division method has significantly decreased to 0.11. This improvement can also be confirmed for the waveform of KMMH16 in Fig. 5. In the result of 0.5–1.0 Hz of the normal method shown in Fig. 5(a), the S-wave initial part of the calculated wave is underestimated for both NS and EW components. In the result of 0.5–1.0 Hz of the division method shown in Fig. 5(b), the calculated wave corresponds well to the observed wave in both components including the S-wave initial part. It is considered that the effect of the division method appears strongly in KMMH16, which is close to the fault and especially affected by high-frequency components. Further, the improvement of the fitting of the S-wave initial part suggests that the idea of setting the slip velocity time function separately for high-frequency and low-frequency is effective, although the assumption of the slip velocity time function is provisional. On the other hand, at a few stations, the residuals of the division method were larger than those of the normal method. At most of these stations, the residual of the fitting for high-frequency component was large in both the normal method and the division method. At these stations, since the accuracy of the shallow ground structure was not good, which contributes significantly to the residual of the fitting. Therefore, it is considered that the effect of the division method did not appear.

Fig. 7 shows a comparison of the observed and theoretical Fourier spectra. For the KMMH16 and KMMH03 with small RSS ratios shown in Fig. 6, it was confirmed that the amplitude of the division method corresponded to the observed value very well compared to one of the normal methods.

From the above results, it is considered that the division method is effective for expanding the frequency band of the waveform inversion.

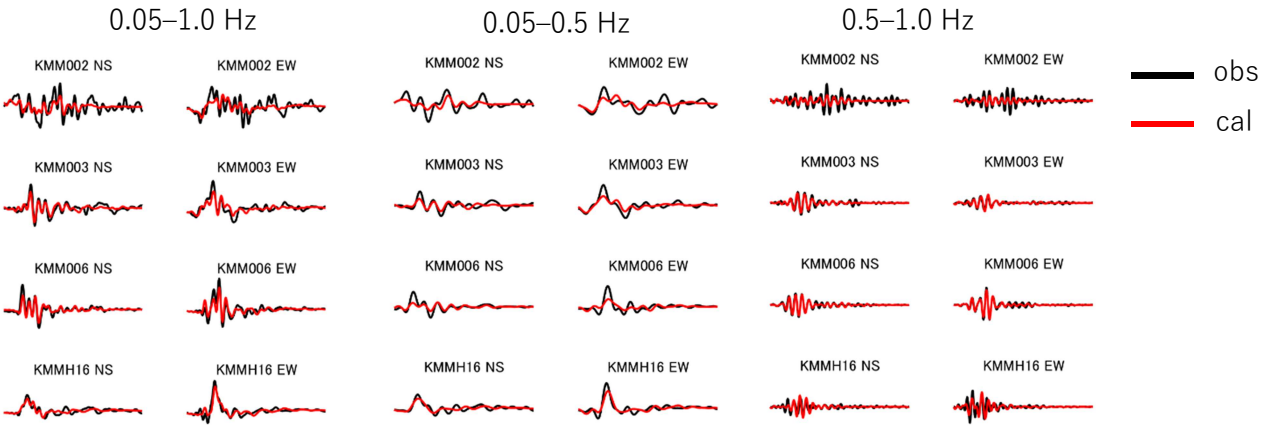

(a) normal method

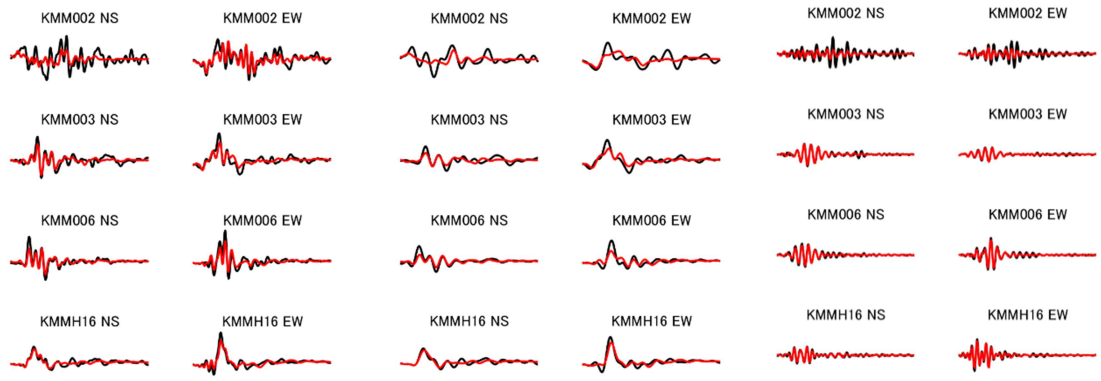

(b) division method

Fig. 5 – Example of fitting observed and calculated waves

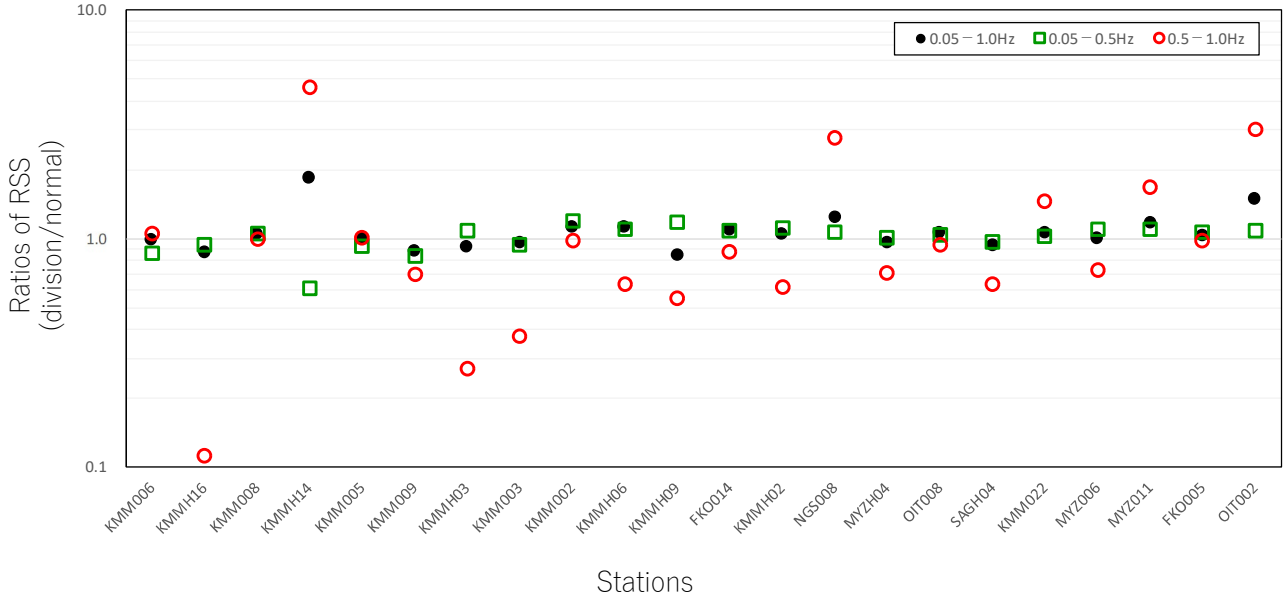

Fig. 6 – Ratio of the residual sum of squares of the division method to the normal method for each station
（arranged from left to right in order of proximity to the hypocenter）

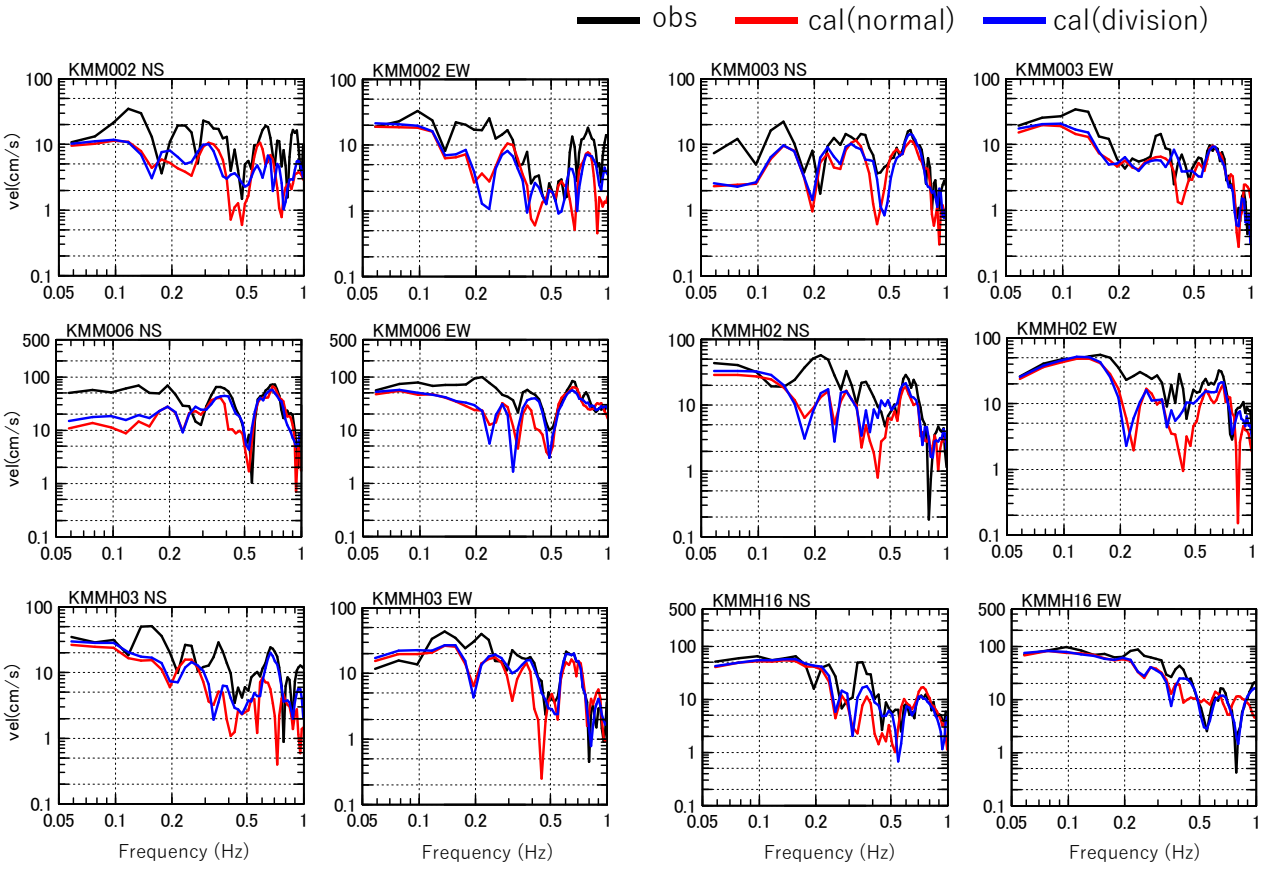

Fig. 7 – Example of comparison of Fourier spectrum

Fig 8 shows a comparison of the fault slip distribution between the normal and the division method in order to examine the effect of the new method on the fault slip distribution. In both methods, a large slip was observed at the Futagawa fault, and there were small differences between the two. Note that there is a difference in slip distribution compared to other studies [8]. One of the reasons is that the rupture velocity was set to be high. However, since we focused only on the effect of the method, we considered that there was no problem in discussing this effect based on the obtained results.

As described above, below 1 Hz, the result of the division method is better than the normal method. Then, the influence of high-frequency was confirmed using the division method. We also examined changes to the fault slip distribution when the upper frequency limit was increased from 0.5 to 1.0 Hz. Specifically, the fault slip distribution studied up to 0.5 Hz by the normal method was compared with the fault slip distribution studied up to 1.0 Hz by the division method. Fig 9 shows the fault slip distributions by both methods. The difference between the slip amount up to 1.0 Hz using the division method and the slip amount up to 0.5 Hz

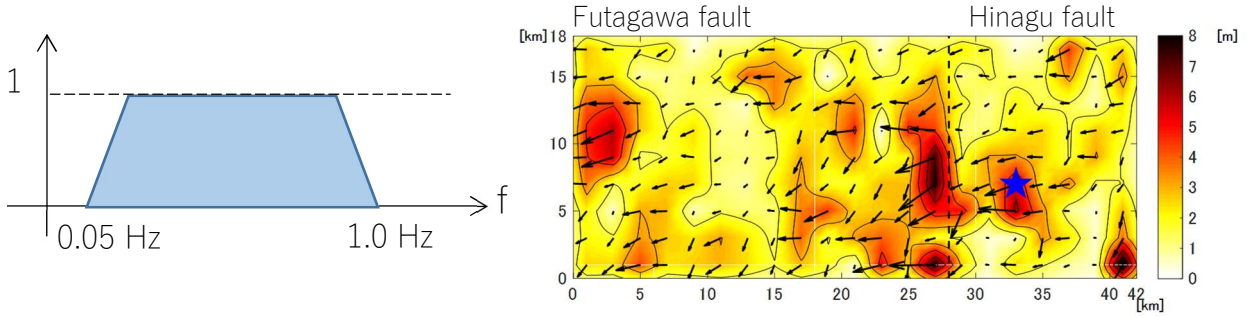

(a) normal method (0.05–1.0 Hz)

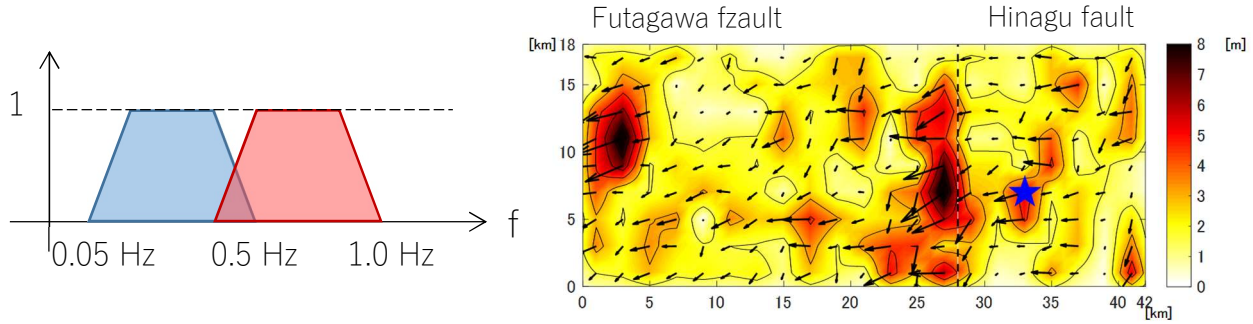

(b) division method (0.05–1.0 Hz)

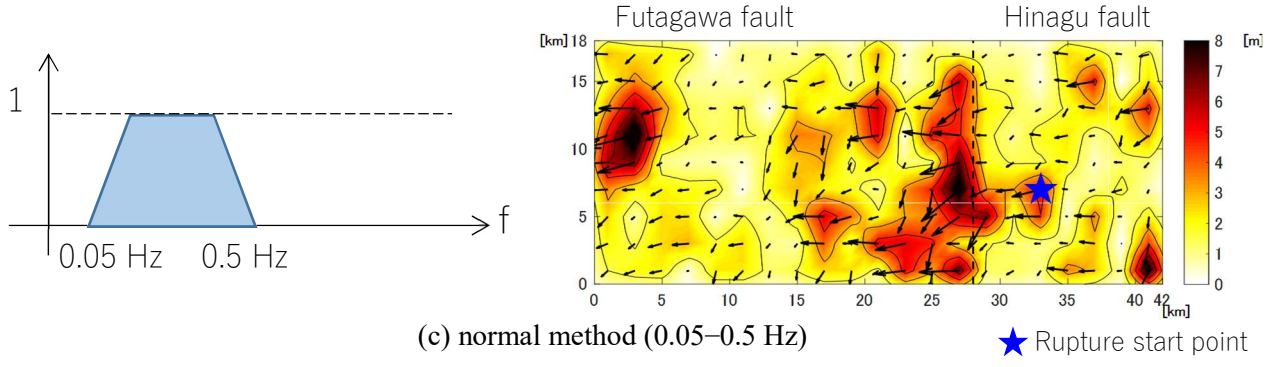

(c) normal method (0.05–0.5 Hz)

Fig. 8 – Fault slip distribution

using the normal method was subtracted, and the difference is shown in Fig. 9. It was observed that when the upper frequency limit was set to 1.0 Hz, the slip was larger around the rupture start point and around the area where the slip was large. In contrast, in the region where the slip was large, there was no difference between the two fault slip amounts. It is suggested that the high frequency component was generated by stopping phases at the point where there were sudden changes to the amount of slip. The characteristics of the relatively high-frequency source region obtained in this study correspond to the findings of Miyake [2].

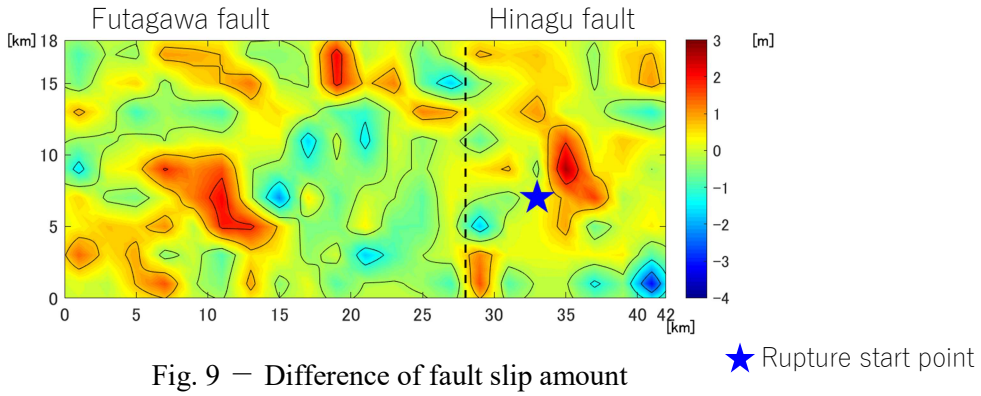

Fig. 9 − Difference of fault slip amount
(b) division method-(c)normal method

5. Conclusion

In this study, we proposed a method to divide frequency analysis and tried to improve the explanation to the observation records up to the high frequency range and estimate of generation area of high-frequency.

In the division method, the residual was found to be smaller compared to the normal method, at most stations near the hypocenter. The division method also provided better results up to the general upper frequency limit of 1 Hz. This confirmed that the division method was effective in waveform inversion.

When using our proposed method, the fault slip was found to be larger around the rupture start point and around the asperity than at low-frequency. This is consistent with previous findings in literature.

In the future, we plan to confirm the applicability of this method to other earthquakes and examine the differences in fault slip distribution at varying frequencies.

6. Acknowledgments

Strong motion data from K-NET, KiK-net were provided by the National Research Institute for Earth Science and Disaster Resilience, Japan. We used the code of the wave number integration method of Professor Yoshiaki Hisada of Kougakuin University to calculate the theoretical Green's function.

7. References

[1] Nakamura H, Miyatake T (2000): An approximate expression of slip velocity time function for simulation of near-field strong ground motion, *Journal of the Seismological Society of Japan. 2nd ser.*, **53** (1), 1-9.
[2] Miyake H (2003): Frequency-dependent source heterogeneities for broadband ground motion simulation. *Ph.D Thesis*, Kyoto University, 105.
[3] Shiba Y (2004): Study on rupture process by waveform inversion using simulated annealing and simulation of broadband ground motions, *CRIEPI REPORT*, N04006, 1-57.
[4] *National Research Institute for Earth Science and Disaster Resilience Kyoshin networks (K-NET, KiK-net)* http://www.kyoshin.bosai.go.jp/kyoshin/.
[5] Hisada Y (1994): An efficient method for computing Green's functions for a layered half-space with sources and receivers at close depths, *Bulletin of the Seismological Society of America*, **84** (5), 1456-1472.

[6] *Japan Seismic Hazard Information Station* http://www.j-shis.bosai.go.jp/.
[7] Umeda N, Sato Y, Kobayashi K (2018): Estimation of underground structure at the KiK-net Mashiki station, Proceedings of *the 15th Japan Earthquake Engineering Symposium*, 188-196. (in Japanese)
[8] Asano K, Iwata T (2016): Source rupture processes of the foreshock and mainshock in the 2016 Kumamoto earthquake sequence estimated from the kinematic waveform inversion of strong motion data, *Earth Planets Space*, **68** (1), 147.
[9] Hartzell SH, Heaton TH (1983): Inversion of strong ground motion and teleseismic waveform data for the fault rupture history of the 1979 Imperial Valley, California, earthquake. *Bulletin of the Seismological Society of America*, **73** (6A), 1553-1583.
[10] Geller RJ (1976): Scaling relations for earthquake source parameters and magnitudes. *Bulletin of the Seismological Society of America*, **66** (5), 1501-1523.